01

Autler-Townes effect of autoionization transition at laser separation of lutetium isotopes

© A.B. D'yachkov, A.A. Gorkunov, S.K. Kovalevich, A.V. Labozin, V.A. Firsov, S.V. Fomichev, G.O. Tsvetkov¶, V.Ya. Panchenko

National Research Center „Kurchatov Institute“,
123182 Moscow, Russia

¶e-mail: Tsvetkov_GO@nrcki.ru

Received July 06, 2023
Revised July 06, 2023
Accepted September 02, 2023

The splitting of the transition from a discrete to an autoionization state, used in a three-step photoionization scheme of lutetium $5d6s^2\,{}^2D_{3/2} - 5d6s6p\,{}^4F^{\circ}_{5/2} - 5d6s7s\,{}^4D_{3/2} - -(53375\,\mathrm{cm}^{-1})^{\circ}_{1/2}$ has been studied. The splitting is proportional to the square root of the intensity, which corresponds to the Autler-Townes effect.

Keywords: autoionization state, photoionization, laser isotope separation.

DOI: 10.61011/EOS.2023.09.57338.5398-23

Introduction

Atomic vapor laser isotope separation (AVLIS) is a method based on selective laser photoionization with several steps of selective photoexcitation being accompanied by a photoionization step that secures the achieved selectivity. The energy of a photoionization radiation quantum may vary within a fairly wide range and should provide photoionization from the higher excited state; however, for selectivity considerations, the quantum energy should not be sufficient for photoionization from intermediate excited states. The photoionization efficiency is specified by this last step, since the cross sections of photoionization to the continuum are normally several orders of magnitude lower than the excitation cross sections of atoms. The use of photoionization via autoionization states (AISs) allows one not only to enhance the efficiency of photoionization, but also to raise its selectivity due to the resonance nature of excitation in AISs. The laser radiation wavelength at the photoionization step and the wavelengths of photoexcitation steps need to be stabilized to a high degree of accuracy in this case.

Autoionization states are used in almost all known photoionization schemes relevant to laser isotope separation. For example, the three-step uranium photoionization scheme [1] $(0\,\mathrm{cm}^{-1} - 17362\,\mathrm{cm}^{-1} - -34659\,\mathrm{cm}^{-1} - 50422\,\mathrm{cm}^{-1})$ features an AIS with an energy of $50422\,\mathrm{cm}^{-1}$, the ytterbium photoionization scheme [2] $0\,\mathrm{cm}^{-1} - 17977\,\mathrm{cm}^{-1} - -35187\,\mathrm{cm}^{-1} - 52346\,\mathrm{cm}^{-1}$ involves an AIS with an energy of $52346\,\mathrm{cm}^{-1}$, neodymium photoionization schemes feature AISs with an energy of 49624 [3] and $50474\,\mathrm{cm}^{-1}$ [4], and an AIS with an energy of $53375\,\mathrm{cm}^{-1}$ [5] is used in three-step lutetium photoionization $(5d6s^2\,{}^2D_{3/2} - 5d6s6p\,{}^4F^{\circ}_{5/2} - 5d6s7s\,{}^4D_{3/2} - -(53375\,\mathrm{cm}^{-1})^{\circ}_{1/2})$. Narrow-band single-mode lasers with a spectral width on the order 150 MHz are required for experiments on separation of ytterbium, neodymium, and lutetium isotopes, and both coherence effects manifested in the splitting of transition lines and the influence of two-photon transitions should be taken into account in this case. These phenomena have been studied extensively [6] for resonance transitions between levels lying below the ionization threshold, but the influence of coherence effects on an AIS lying above the photoionization threshold remains barely investigated. Our interest was drawn to AISs in a strong field by the discovery of an ion yield reduction with an increase in power at the third (last) ionization step in experiments on saturation [7]. This may be viewed as a sign that the contribution of radiative decay becomes more significant compared to the ionization channel. Note, however, that the mentioned reduction is observed at intensities well above those corresponding to the point where ionization reaches saturation. In the present study, the influence of coherence effects on the autoionization transition is examined experimentally, and a numerical model for comparison with the obtained data is proposed.

Studies into AISs in a laser field have been initiated on the cusp of the 1980s due, apparently, to the emergence of possibilities for multiphoton excitation of atoms for the purpose of laser separation of isotopes and to generation (laser generation included [8–10]) of tunable radiation in the ultraviolet (UV) and vacuum UV regions. The research into autoionization-like resonances (laser-induced continuum structure, LICS) published at the time [11] has also contributed to an increase in interest in AISs. The limited availability of radiation sources dictated that studies were first confined to the optical and near UV ranges (excitation energy < 10 eV), but the development of short-wave high-power light sources with ultrashort pulses

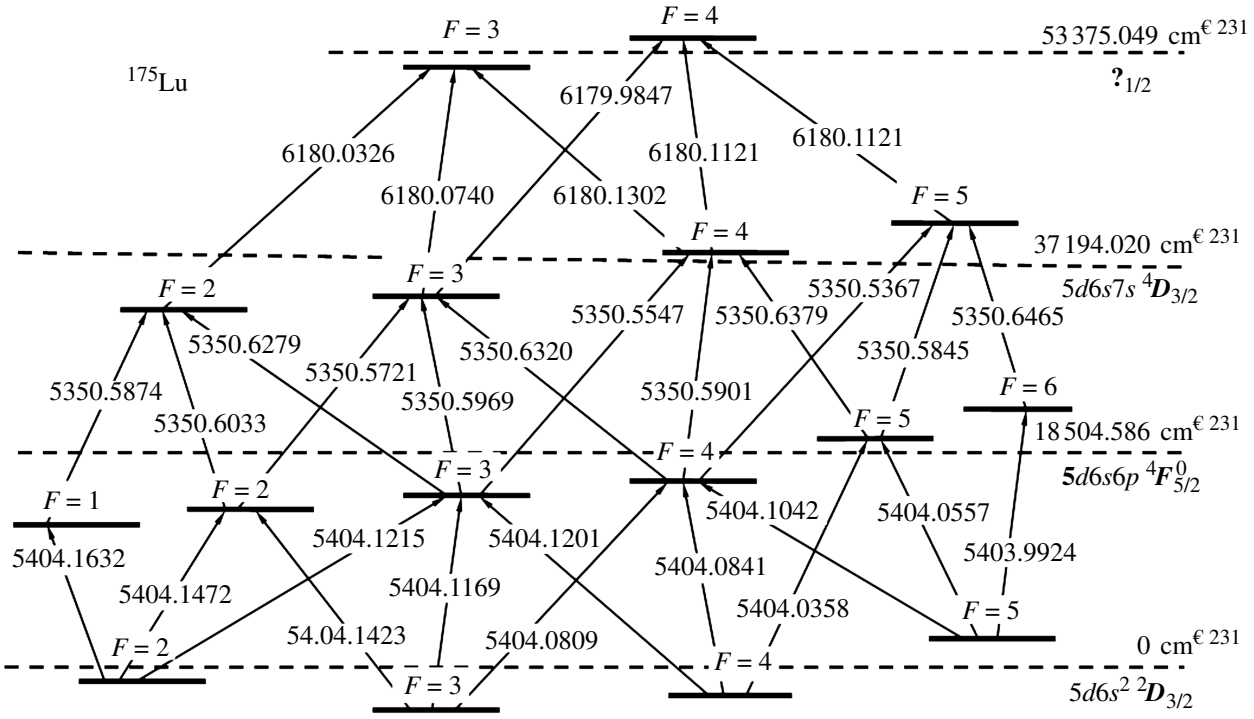

Figure 1. Optical diagram of ^{175}Lu ($I = 7/2$) photoionization (the wavelengths are vacuum ones, Å) [5].

(higher optical harmonics, free-electron lasers) initiated a shift toward highly excited states (several tens of eV and above) in research into atomic continuum states. This opened up the opportunities for examination of AISs of atoms with a high ionization potentials, such as He, Ne, and Ar, with a fine temporal resolution [12–16].

In a laser step photoionization scheme, an atom undergoes a transition to an AIS upon absorption of a photon from a discrete state lying below the ionization threshold. Owing to the Coulomb interelectron interaction, AISs, in contrast to common coupled atomic states, may ionize spontaneously to the one-electron continuum, and the AIS width is a combination of the widths of decay into an ionized state and spontaneous radiative decay. Typical ionization widths, which exceed $10^{13}\,s^{-1}$ in this case, are much greater than the radiative widths of discrete levels ($10^8 - 10^9\,s^{-1}$), and an atom entering an AIS normally gets ionized. The AIS decay to the continuum and the direct field ionization of an atom interfere if the final states of these processes match. The photoionization resonance thus acquires an asymmetric Fano profile [17]. This scenario is altered significantly in a strong laser field, and the photoionization resonance profile and the spectrum of produced photoelectrons may change markedly as a result. Owing to the presence of a radiative channel, oscillations between an AIS and the lower state (dynamical Stark effect) emerge when the Rabi frequency becomes comparable to the AIS decay width or exceeds it. This leads, among other things, to splitting of the autoionization resonance and, under certain conditions, to its narrowing down to radiative widths [10,18–20]. It has been predicted theoretically in [10] that a strong field at an autoionization resonance may stabilize an AIS against decay to the continuum as a result of destructive interference between ionization and the radiative AIS decay. The influence of a strong laser field on transitions between coupled states lying below the ionization threshold has been discovered long ago. The authors of [21] were the first to demonstrate experimentally the dynamical Stark effect for two AISs in the continuum. It was found that this effect suppresses photoionization to a significant degree. We managed to find only one published experimental study [22] that dealt, although only implicitly, with transitions from a coupled state below the ionization threshold to two AISs. With the intensity reaching a fairly significant level of $10^9\,W/cm^2$, the Autler–Townes splitting magnitude was $7.5\,cm^{-1}$ at one of the transitions, while the other revealed no effect of this kind. The present study is also focused on the transition to an AIS from a coupled preionization state under the influence of a strong laser field in the lutetium photoionization scheme (Fig. 1).

It can be seen from Fig. 1 that the magnitude of hyperfine splitting of levels of the photoionization diagram is normally much greater than the spectral width of laser radiation (100–150 MHz). Therefore, with the wavelengths tuned in a certain way, photoionization may proceed in a single channel only: a certain combination of hyperfine structure (HFS) components of the ground, the first and the second excited, and the autoionization states, which are specified by the values of total angular momentum F_i ($F_0 \to F_1 \to F_2 \to F_3$) of an atom. In order to minimize

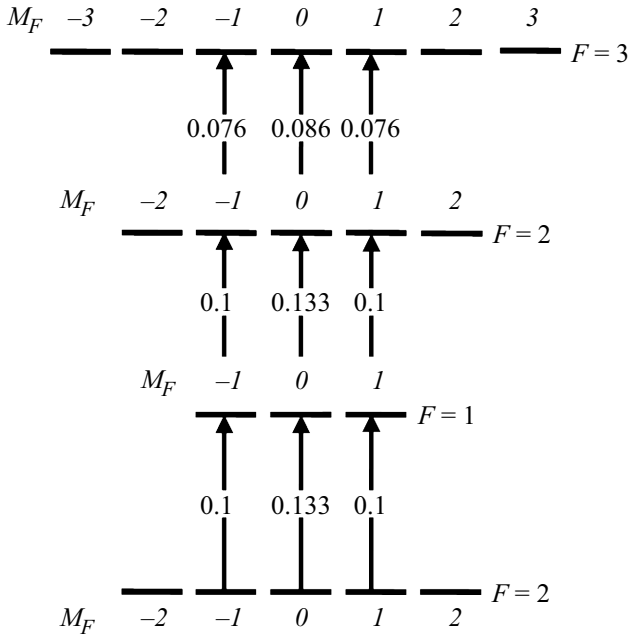

Figure 2. Diagrams of transitions between projections in the 2-1-2-3 channel. The values of the matrix element of the transition dipole moment are indicated at arrows.

the potential spread of Rabi frequencies due to transitions between different projections of total angular momentum M_F, the $2-1-2-3$ channel was chosen for experimental studies. If linearly polarized laser radiation is used, selection rule $\Delta M_F = 0$ then applies to total angular momentum projections M_F , and transitions involving projections -1, 0, and 1 are allowed (Fig. 2). Matrix elements of the dipole moment of transitions (indicated at arrows in Fig. 2) involving projections -1 and 1 match and differ insignificantly from the value for projection 0 for the third transition.

Experiment

The AIS splitting in ^{175}Lu (its natural abundance is 96.4%) in the $5d6s^2\,{}^2D_{3/2} - 5d6s6p\,{}^4F^{\circ}_{5/2} - -5d6s7s\,{}^4D_{3/2} - (53375\,\mathrm{cm}^{-1})^{\circ}_{1/2}$ photoionization scheme was examined by laser resonance ionization mass spectrometry (LRIMS). Radiation produced by three pulsed single-mode dye lasers (DLs) pumped by copper vapor lasers was used for resonance excitation and ionization of atoms. The spectral width of the DL lasing line was 100–150 MHz (FWHM), the pulse duration (FWHM) was 20 ns, the pulse repetition rate was 10 kHz, and the emission of all three lasers was polarized linearly in the same direction. Laser pulses of the second and the third steps were aligned in time and shifted by 20 ns relative to the first step (the lifetime of the first excited state $5d6s6p\,{}^4F^{\circ}_{5/2}$ is 472 ns [23]). An MS-7302 commercial mass spectrometer was used to detect photoions; experiments were performed with a narrow atomic beam (with Doppler broadening ~ 150 MHz). The technical parameters and features of the experimental setup were characterized in detail in [4,24].

In experiments, DL 1 with a mean power density of 48 mW/cm^2 (an intensity of 240 W/cm^2) was tuned in resonance with the first transition. The wavelength of DL 3 was tuned in resonance with the transition to an AIS with an energy of 53375 cm^{-1}; the DL 3 intensity varied within the 20–150 kW/cm^2 range. The intensity of DL 2 was reduced to 10 W/cm^2, and its wavelength was scanned as a probe in the region of the second transition resonance at a constant DL 3 intensity. The variation of photoion current in the process of DL 2 wavelength scanning in the region of the second transition resonance at a DL 3 intensity of 118.5 kW/cm^2 is presented in Fig. 3. Figure 4 presents the dependence of splitting on the DL 3 radiation intensity. Experimental data agree closely with the model assuming that the splitting magnitude is proportional to the square root of intensity.

Theoretical modeling of experimental data

A simplified model of two-photon ionization of an atom via AIS 3, which is shown schematically in Fig. 5, was used to model the obtained results of experiments. Owing to time delays set in the experiments, the atomic system

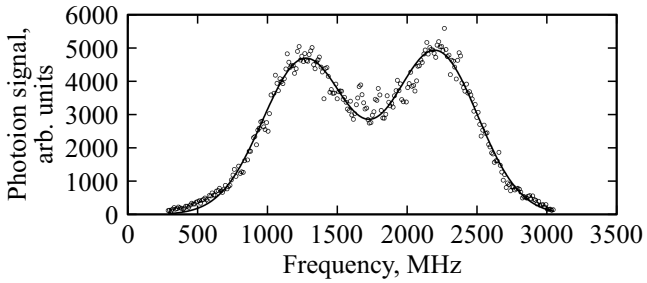

Figure 3. Dependence of the photoion signal on the laser radiation frequency at the second step. The mean radiation power density at the third step is 23.7 W/cm^2 (the intensity is 118.5 kW/cm^2).

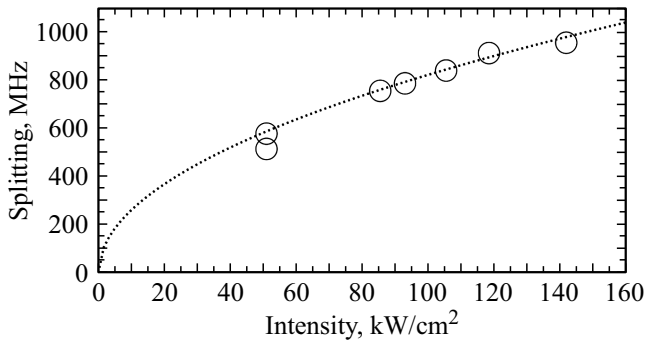

Figure 4. Dependence of splitting on intensity I of laser radiation at the third step. Circles denote experimental data. The dashed curve represents variation $\sim \sqrt{I}$.

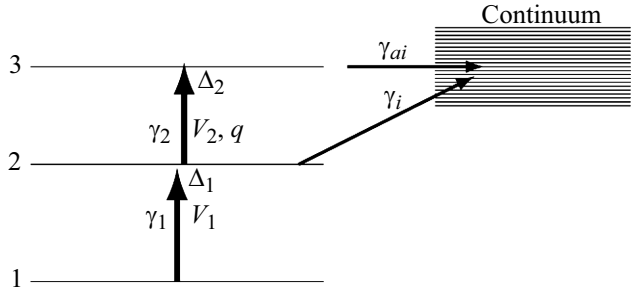

Figure 5. Diagram of two-photon ionization of an atom via an AIS corresponding to the calculation model and Eqs. (1)–(7).

was affected simultaneously by laser radiation of the second and the third steps. Therefore, a four-level system was substituted in the numerical model by a three-level one with its initial state being the first excited $5d6s6p\,^4F^{\circ}_{5/2}$ state populated by a laser pulse of the first step. Lower 1 and upper 2 photoexcitation steps in this model scheme (Fig. 5) correspond to the second and the third steps of experimental photoionization; notably, we assume that the first excited level with $F = 1$ (corresponding to lower level 1 in Fig. 5) is degenerate in momentum F projections (over which averaging is performed). The excitation and subsequent ionization of an atom in this model may be characterized by the following system of equations for density matrix $\rho_{ij}(i, j = 1, 2, 3)$ that was derived in [25]:

$$i\frac{\partial\rho_{11}}{\partial t} = -\frac{V_1^*}{2}\rho_{21} + \frac{V_1}{2}\rho_{12} + i\gamma_1\rho_{22}, \tag{1}$$

$$i\frac{\partial\rho_{22}}{\partial t} = -\frac{V_1}{2}\rho_{12} + \frac{V_1^*}{2}\rho_{21} - \frac{V_2^*}{2}\left(1 - \frac{i}{q}\right)\rho_{32} + \frac{V_2}{2}\left(1 + \frac{i}{q}\right)\rho_{23} - i(\gamma_1 + \gamma_i)\rho_{22} + i\gamma_2\rho_{33}, \tag{2}$$

$$i\frac{\partial\rho_{33}}{\partial t} = -\frac{V_2}{2}\left(1 - \frac{i}{q}\right)\rho_{23} + \frac{V_2^*}{2}\left(1 + \frac{i}{q}\right)\rho_{32} - i(\gamma_2 + \gamma_{ai})\rho_{33}, \tag{3}$$

$$i\frac{\partial\rho_{21}}{\partial t} = -\left(\Delta_1 + \frac{i}{2}(\gamma_1 + \gamma_i) + 2i\Delta_{L1}\right)\rho_{21} - \frac{V_1}{2}(\rho_{11} - \rho_{22}) - \frac{V_2^*}{2}\left(1 - \frac{i}{q}\right)\rho_{31}, \tag{4}$$

$$i\frac{\partial\rho_{32}}{\partial t} = -\left(\Delta_2 + \frac{i}{2}(\gamma_1 + \gamma_2 + \gamma_i + \gamma_{ai}) + 2i\Delta_{L2}\right)\rho_{32} - \frac{V_2}{2}\left(\left(1 - \frac{i}{q}\right)\rho_{22} - \left(1 + \frac{i}{q}\right)\rho_{33}\right) + \frac{V_1^*}{2}\rho_{31}, \tag{5}$$

$$i\frac{\partial\rho_{31}}{\partial t} = -\left(\Delta_1 + \Delta_2 + \frac{i}{2}(\gamma_2 + \gamma_{ai}) + 2i(\Delta_{L1} + \Delta_{L2})\right)\rho_{31} - \frac{V_2}{2}\left(1 - \frac{i}{q}\right)\rho_{21} + \frac{V_1}{2}\rho_{32}, \tag{6}$$

$$\rho_i = 1 - \rho_{11} - \rho_{22} - \rho_{33}. \tag{7}$$

Here, ρ_i is the sought-for degree of ionization of an atom after its excitation by two laser pulses, and the equations for density matrix elements ρ_{12}, ρ_{23}, and ρ_{13} are complex conjugate to Eqs. (4), (5), and (6), respectively. The value of $\rho_{11}(t = 0) = 1$ and zero values of all the other density matrix elements were the initial conditions for solving this system of equations at time point $t = 0$.

Quantities $\Delta_1 = \omega_1 - \omega_{01}$ and $\Delta_2 = \omega_2 - \omega_{02}$ in these equations are the magnitudes of frequency detuning of laser radiation at the lower and upper excitation steps from the corresponding resonance frequencies $\omega_{0k} = 2\pi\nu_{0k}$ $(k = 1, 2)$. In the present case, $\nu_{01} = 5.6029 \cdot 10^{14}$ Hz and $\nu_{02} = 4.8507 \cdot 10^{14}$ Hz (equivalent to 18690 and 16181 cm^{-1}, respectively). Quantities $V_1 = d_1E_1/\hbar \sim \sqrt{I_1}$ and $V_2 = d_2E_2/\hbar \sim \sqrt{I_2}$ are Rabi frequencies defined by the matrix elements of the operator of interaction between resonance radiation and an atom at the corresponding transitions, which are assumed to be real (if resonance radiation is linearly polarized) and be proportional to the square root of the corresponding laser radiation intensities I_1 and I_2; d_1 and d_2 are the dipole moments of resonance transitions; and $\gamma_1 = 1/\tau_1$ and $\gamma_2 = 1/\tau_2$ are their homogeneous radiative widths (inverse spontaneous relaxation times or Einstein coefficients). Squared absolute values of the dipole moment for a transition with certain total angular momentum values F and F' are written in terms of Wigner $3j$ and $6j$ symbols as [26]

$$|d_{FF'}|^2 = (2F+1)(2F'+1)\overline{\begin{pmatrix} F & 1 & F' \\ -M & 0 & M' \end{pmatrix}^2} \times \times \begin{Bmatrix} -J & 1 & J' \\ F' & I & F \end{Bmatrix}^2 |\langle J \parallel D \parallel J' \rangle|^2, \tag{8}$$

where the bar denotes averaging over transitions with different values (0 or ± 1) of projections of moment M and M' at $\Delta M = M - M' = 0$ (Fig. 2), J and J' are the quantum numbers of total orbital and spin moments of electrons, and $I = 7/2$ is the nuclear spin of lutetium. Since γ_1 and γ_2 are defined by the same reduced dipole matrix elements of transitions $\tilde{d} = \langle J \parallel D \parallel J' \rangle$ as $\gamma_k = 4\omega_{0k}^3|\tilde{d}_k|^2/\{3(2J'+1)\hbar c^3\}$ (at $k = 1, 2$), the relation between quantities γ_1 and γ_2 and Rabi frequencies in the used simplest model of non-degenerate transitions may be written as $V_k^2 = \gamma_k\omega_{0k}(I_k/I_{0k})$, where $I_k = cE_k^2/(8\pi)$ is the laser radiation intensity at step k, $I_{0k} = \hbar\omega_{0k}^4/(6\pi c^2 f_k)$, and

$$f_k = (2J'+1)(2F+1)(2F'+1)\overline{\begin{pmatrix} F & 1 & F' \\ -M & 0 & M' \end{pmatrix}^2} \times \times \begin{Bmatrix} -J & 1 & J' \\ F' & I & F \end{Bmatrix}^2. \tag{9}$$

In the present case, $f_1 = 2/9$ (at $F = 1$, $F' = 2$, $J = 5/2$, $J' = 3/2$) and $f_2 = 25/126$ (at $F = 2$, $F' = 3$, $J = 3/2$, $J' = 1/2$); $I_{01} = 4.3 \cdot 10^6$ W/cm^2; and $I_{02} = 2.7 \cdot 10^6$ W/cm^2. Quantity $\gamma_i = \sigma_i I_2/(\hbar\omega_{02})$ is the

ionization width of intermediate level 2 that is proportional to cross section σ_i of direct photoionization from level 2 and intensity I_2 of laser radiation of the upper step. Quantity γ_{ai} is the width of autoionization level 3 associated with transitions from this level directly to the continuum, and q is the Fano parameter of the transition to autoionization state 3 from discrete atomic state 2 to which the photoionization resonance curve asymmetry is attributable. Parameter q characterizes the ratio of probability amplitudes of the photoionization transition via a discrete state and the direct transition to the continuum spectrum [25]. In the context of the present study, it may be regarded as a phenomenological parameter that is adjusted to achieve the closest fit between calculated and experimental data. Asymmetry vanishes in the $|q| \gg 1$ limit. Note that the ionization width for the direct transition to the continuum spectrum at typical values of the photoionization cross section ($\sigma_i \sim 10^{-17}\,\mathrm{cm}^2$) is $\gamma_i[\mathrm{s}^{-1}] \sim 10^2 \times I_2\,[\mathrm{W/cm}^2]$ and has only a minor influence on the shape of photoionization resonance curves. Finally, quantities Δ_{L1} and Δ_{L2} in Eqs. (4)–(6) are the homogeneous Lorentzian widths of lasing spectra at the first and the second steps, respectively. Fitting of the experimental data was performed in two ways: with zero broadening of lasing spectra ($\Delta_{L1} = \Delta_{L2} = 0$) and with equal nonzero values of 30 MHz (according to various sources, this is close to the spectral width of laser radiation in a single pulse [27]) corresponding to spectra broadenings $\tilde{\Delta}_{L1} = \Delta_{L1}/(2\pi)$ and $\tilde{\Delta}_{L2} = \Delta_{L2}/(2\pi)$.

In the course of modeling of the photoionization process, detuning Δ_1 from resonance of the lower excitation step (or, equivalently, laser frequency ν_1) was scanned within a wide range, while $\Delta_2 = 0$ was set for the upper excitation step. At the lower excitation step, laser radiation intensity I_1 was chosen from within the $5-13\,\mathrm{W/cm}^2$ range (in order to avoid complete saturation in photoionization), and Einstein coefficient $\gamma_1 = 8.7 \cdot 10^7\,\mathrm{s}^{-1}$ (with $\tilde{\gamma_1} = \gamma_1/(2\pi) = 13.85\,\mathrm{MHz}$), which corresponds to experimental lifetime $\tau_1 = 11.5\,\mathrm{ns}$ of state 2, was set. Calculations were performed for two rectangular synchronized laser pulses of the lower and upper steps with duration $\tau_{\mathrm{puls}} = 20\,\mathrm{ns}$ (note that photoionization calculations were extended beyond the duration of pulses in order to take all ions produced as a result of photoionization into account). The remaining three quantities, namely, γ_2, γ_{ai}, and q, were adjustable parameters. The first two parameters played a leading part in fitting of the experimental data (see Fig. 4), while asymmetry parameter q was adjusted so as to make the asymmetric experimental resonance curves (similar to those in Fig. 3) match visually the calculated ones. The closest quantitative agreement between experimental and calculated data in terms of resonance splitting and qualitative agreement of the resonance curves themselves was provided by the model with $q = 7$ and the following values of the other adjustable parameters: in the case of zero laser widths, $\gamma_2 = 2.82 \cdot 10^5\,\mathrm{s}^{-1}$ and $\gamma_{ai} = 3.40 \cdot 10^9\,\mathrm{s}^{-1}$ ($\tilde{\gamma}_2 = 4.5 \cdot 10^4$ Hz and $\tilde{\gamma}_{ai} = 500$ MHz); in the case of laser widths corresponding to 30 MHz, $\gamma_2 = 2.82 \cdot 10^5\,\mathrm{s}^{-1}$ and $\gamma_{ai} = 1.63 \cdot 10^9\,\mathrm{s}^{-1}$ ($\tilde{\gamma}_2 = 4.5 \cdot 10^4$ Hz and $\tilde{\gamma}_{ai} = 260$ MHz).

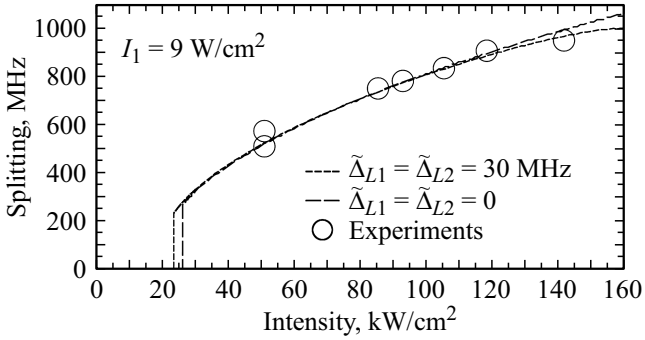

Figure 6. Results of calculation of splitting of photoionization curve peaks as a function of laser intensity I_2 at laser radiation intensity $I_1 = 9\,\mathrm{W/cm}^2$ for the lower step and laser widths set to 0 or 30 MHz. The experimental data for comparison were taken from Fig. 4.

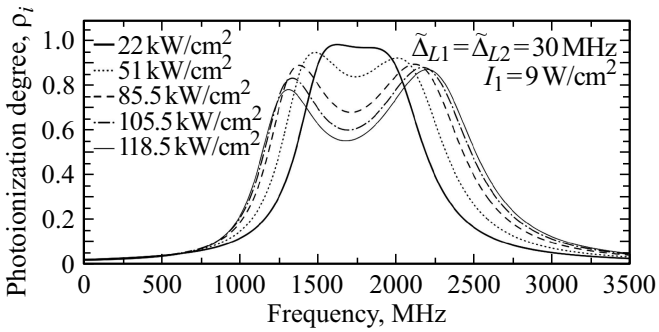

Figure 7. Results of calculation of photoionization degree ρ_i at laser widths of 30 MHz for several different intensities of laser radiation of the upper step I_2 (indicated in the figure) and at intensity $I_1 = 9\,\mathrm{W/cm}^2$ of laser radiation of the lower step.

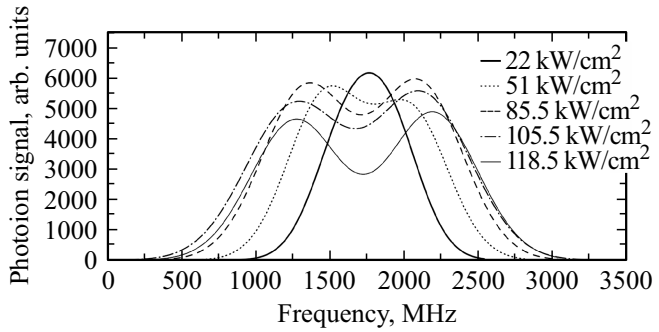

Figure 8. Experimental photoion signal at different intensities of laser radiation of the third step (indicated in the figure) that excites an AIS.

The variations of splitting of the photoionization curve with intensity I_2 of laser radiation of the upper step that were determined in experiments and calculated

with the model parameters indicated above and intensity $I_1 = 9\,\mathrm{W/cm^2}$ are presented in Fig. 6. Note that the results of calculation of resonance splitting depend only weakly on intensity I_1 of laser radiation of the first step within the considered range of its values. Ionization curves were calculated as functions of detuning Δ_1 (Fig. 7) for certain specific intensities I_2 of laser radiation of the upper step that were probed experimentally. The corresponding experimental data for comparison are presented in Fig. 8.

The obtained results suggest that the dependence of resonance splitting on laser radiation intensity I_2 may be characterized equally well with different sets of adjustable parameters (in the present case, with different widths of laser radiation at two excitation steps). In both cases, the effect of emergence of two peaks in the photoionization curve (i.e., formation of a dip at its center) is threshold in nature: a certain finite splitting magnitude emerges at a specific nonzero laser radiation intensity I_2, which is approximately equal to $25\,\mathrm{kW/cm^2}$ in the present study. The magnitude of splitting below this intensity is zero (this corresponds to the experiment at intensity $I_2 = 22\,\mathrm{kW/cm^2}$ with a nascent kink in the resonance curve seen instead of the double-peak structure). However, it appears that this threshold property of the Autler–Townes effect should not be specific to the resonance involving an AIS (i.e., should be universal in nature).

It follows from the results of visual comparison of experimental data and photoionization curves calculated as functions of the laser frequency at the lower excitation step that a fine semi-quantitative agreement with regard to valleys between peaks, peak asymmetry, and the overall width of curves is provided by the second set of adjustable parameters obtained for a nonzero (30 MHz) laser radiation width (Fig. 7).

As for the asymmetry of photoionization curves, it is worth mentioning that this asymmetry is associated not just with Fano parameter q of an AIS (when q is substituted by $-q$, asymmetry inversion occurs), but also with nonzero detuning Δ_2 of the upper-step laser from resonance (a Δ_2 sign change also causes asymmetry inversion). Although the laser of the upper excitation step was tuned right to the transition center, which corresponds to $\Delta_2 = 0$, in the experiment, detuning Δ_2 for individual pulses may fluctuate in the course of multipulse excitation of the atomic system. However, averaging over a large number of pulses should ensure that the end result corresponds to $\Delta_2 \equiv 0$. The possible shift of the resonance frequency of the upper transition, which depends on intensity I_2 of laser radiation of the upper step, may produce a more significant effect. The combined influence of two asymmetry mechanisms may potentially lead to a change in the character of asymmetry of photoionization curves under laser intensity I_2 variations. This is exactly what is observed both in the experimental data in Figs. 4 and 8 and in the theoretical results in Fig. 7 corresponding to a nonzero laser radiation width and intensity $I_1 = 9\,\mathrm{W/cm^2}$ of laser radiation of the lower step. Note that the character of asymmetry did not vary with laser radiation intensity I_2 at lower values of intensity I_1 (e.g., at $I_1 = 5\,\mathrm{W/cm^2}$). These fine effects warrant a separate study and are not examined in detail here. All in all, the obtained modeling data suggest that the Autler–Townes effect should manifest itself in excitation of atoms and/or molecules to AISs in much the same fashion as in common processes of their excitation and ionization via discrete coupled states.

Conclusions

Thus, when conducting isotopically selective photoionization by narrow-band single-mode lasers with the use of AISs, one should make an allowance for possible splitting of an AIS, which does not differ in this regard from any other resonance state in the photoionization scheme. This splitting manifests itself in practice as a reduction in the photoion signal intensity of the target isotope that occurs when the intensity of laser radiation of the last ionization step increases. This effect should be the most pronounced for „weak" AISs with low γ_{ai} values; a coordinated enhancement of intensity of laser radiation at all steps of the photoionization scheme may be needed in this case to equalize the Rabi frequencies.

The results of calculations for the examined photoionization scheme with a $53375\,\mathrm{cm^{-1}}$ AIS agree most closely with the experimental data at the following values of adjustable parameters: $\tilde{\gamma}_{ai} = 260\,\mathrm{MHz}$, $\tilde{\gamma}_2 = 4.5 \cdot 10^4\,\mathrm{Hz}$, and Fano parameter $q = 7$. Splitting reveals itself at third-step intensities above $25\,\mathrm{kW/cm^2}$, while the typical intensities used in selective photoionization are $15-30\,\mathrm{kW/cm^2}$.

When calculating the efficiency and selectivity of photoionization with the use of AISs, one should regard an AIS as a resonance level lying below the ionization threshold with ionization with constant γ_{ai} taking on the role of decay to the coupled state. The sole difference is in the fact that an AIS features Fano parameter q, which characterizes the channel of direct photoionization to the continuum from a pre-ionization state. With the problem posed this way, additional selectivity induced by an AIS may be taken into account, and a most complete description of the process of selective photoionization may be obtained.

Funding

The study was supported by a grant from the Russian Science Foundation (project No. 17-13-01180).

Conflict of interest

The authors declare that they have no conflict of interest.

References

[1] P.T. Greenland, D.N. Travis, D.J.H. Wort. J. Phys. B, **23**(17), 2945 (1990). DOI: 10.1088/0953-4075/23/17/007

[2] S.I. Yakovlenko. Quant. Electron., **28**(11), 945 (1998). DOI: 10.1070/QE1998v028n11ABEH001364.

[3] A.P. Babichev, I.S. Grigoriev, A.I. Grigoriev, A.P. Dorovskii, A.B. D'yachkov, S.K. Kovalevich, V.A. Kochetov, V.A. Kuznetsov, V.P. Labozin, A.V. Matrakhov, S.M. Mironov, S.A. Nikulin, A.V. Pesnya, N.I. Timofeev, V.A. Firsov, G.O. Tsvetkov, G.G. Shatalova. Quant. Electron., **35**(10), 879 (2005). DOI: 10.1070/QE2005v035n10ABEH006601.
[4] A.B. D'yachkov, A.A. Gorkunov, A.V. Labozin, S.M. Mironov, V.Ya. Panchenko, V.A. Firsov, G.O. Tsvetkov. Quant. Electron., **48**(1), 75 (2018). DOI: 10.1070/QEL16493.
[5] I.V. Ageeva, A.B. D'yachkov, A.A. Gorkunov, A.V. Labozin, S.M. Mironov, V.Ya. Panchenko, V.A. Firsov, G.O. Tsvetkov, E.G. Tsvetkova. Quant. Electron., **49**(9), 832 (2019). DOI: 10.1070/QEL17049.
[6] B. Shore. Acta Phys. Slovaca. Rev. Tutorials, **58**(3), 243 (2008).
[7] A.B. D'yachkov, A.A. Gorkunov, A.V. Labozin, K.A. Makoveeva, S.M. Mironov, V.A. Firsov, G.O. Tsvetkov, V.Ya. Panchenko. Radiochemistry, **64**(1), 49 (2022). DOI: 10.1134/S1066362222010088.
[8] J. Bokor, R.R. Freeman, W.E. Cooke. Phys. Rev. Lett., **48**(18), 1242 (1982). DOI: 10.1103/PhysRevLett.48.1242
[9] C.K. Rhodes. *VUV and XUV Generation with Multiphoton Excitation, in Int. Quant. Electron. Conf., H. Koglnik, Y. Shen, M. Richardson, C. Tang, eds., OSA Technical Digest* (Optica Publishing Group, 1984), p. WLL2. https://opg.optica.org/abstract.cfm?URI=IQEC-1984-WLL2
[10] P. Lambropoulos, P. Zoller. Phys. Rev. A, **24**(1), 379 (1981). DOI: 10.1103/PhysRevA.24.379
[11] Yu.I. Geller, A.K. Popov. Sov. J. Quantum Electron., **6**(5), 606 (1976). DOI: 10.1070/QE1976v006n05ABEH011378.
[12] N. Harkema, C. Cariker, E. Lindroth, L. Argenti, A. Sandhu. Phys. Rev. Lett., **127**(2), 023202 (2021). DOI: 10.1103/PhysRevLett.127.023202
[13] S.I. Themelis, P. Lambropoulos, M. Meyer. J. Phys. B, **37**(21), 4281 (2004). DOI: 10.1088/0953-4075/37/21/005
[14] V. Gruson, L. Barreau, Á Jiménez-Galan, F. Risoud, J. Caillat, A. Maquet, B. Carré, F. Lepetit, J.-F. Hergott, T. Ruchon, L. Argenti, R. Taïeb, F. Martín, P. Saliéres. Science, **354**(6313), 734 (2016). DOI: 10.1126/science.aah5188
[15] Z.-H. Loh, C.H. Greene, S.R. Leone. Chem. Phys., **350**(1−3), 7 (2008). DOI: 10.1016/j.chemphys.2007.11.005
[16] M. Isinger, R.J. Squibb, D. Busto, S. Zhong, A. Harth, D. Kroon, S. Nandi, C.L. Arnold, M. Miranda, J.M. Dahlström, E. Lindroth, R. Feifel, M. Gisselbrecht, A. L'Huillier. Science, **358**(6365), 893 (2017). DOI: 10.1126/science.aao7043
[17] U. Fano. Phys. Rev., **124**(6), 1866 (1961). DOI: 10.1103/PhysRev.124.1866
[18] Yu.I. Heller, A.K. Popov. Phys. Lett. A, **56**(6), 453 (1976). DOI: 10.1016/0375-9601(76)90725-8
[19] A.I. Andryushin, A.E. Kazakov, M.V. Fedorov. JETP, **55**(1), 53 (1982).
[20] A.I. Andryushin, A.E. Kazakov, M.V. Fedorov. JETP, **61**(4), 678 (1985).
[21] N.E. Karapanagioti, O. Faucher, Y.L. Shao, D. Charalambidis, H. Bachau, E. Cormier. Phys. Rev. Lett., **74**(13), 2431 (1995). DOI: 10.1103/PhysRevLett.74.2431
[22] O. Faucher, Y.L. Shao, D. Charalambidis, C. Fotakis. Phys. Rev. A, **50**(1), 641 (1994). DOI: 10.1103/PhysRevA.50.641
[23] J.A. Fedchak, E.A. Den Hartog, J.E. Lawler, P. Palmeri, P. Quinet, E. Biémont. Astrophys. J., **542**(2), 1109 (2000). DOI: 10.1086/317034
[24] A.B. D'yachkov, A.A. Gorkunov, A.V. Labozin, S.M. Mironov, V.Ya. Panchenko, V.A. Firsov, G.O. Tsvetkov. Instr. Exp. Tech., **61**(4), 548 (2018). DOI: 10.1134/S0020441218040048
[25] A. Boeglin, B. Fain, S.-H. Lin. J. Chem. Phys., **84**(9), 4838 (1986). DOI: 10.1063/1.449973
[26] A.B. D'yachkov, A.A. Gorkunov, A.V. Labozin, S.M. Mironov, V.A. Firsov, G.O. Tsvetkov, V.Ya. Panchenko. Quant. Electron., **52**(4), 367 (2022). DOI: 10.1070/QEL18029.
[27] A.B. D'yachkov, A.A. Gorkunov, A.V. Labozin, S.M. Mironov, V.A. Firsov, G.O. Tsvetkov, V.Ya. Panchenko. Bull. Lebedev Physics Institute, Vol. 50, Suppl. 2, pp. S187−S193 (2023). DOI: 10.3103/S106833562314004X

Translated by D.Safin